JOURNAL OF MATERIALS PROCESSING TECHNOLOGY 207 (2008) 271–275

journal homepage: www.elsevier.com/locate/jmatprotec

Microstructure study of laser welding cast nickel-based superalloy K418

Ming Pang, Gang Yu, Heng-Hai Wang, Cai-Yun Zheng*

Laboratory for Laser Intelligent Manufacturing, Institute of Mechanic, Chinese Academy of Sciences, 15 Beisihuanxi Road, Beijing 100080, PR China

ARTICLE INFO

Article history:
Received 10 June 2007
Received in revised form
21 November 2007
Accepted 21 December 2007

Keywords:
Nickel-based superalloy
Needle carbides
Cracks

ABSTRACT

Experiments of laser welding cast nickel-based superalloy K418 were conducted. Microstructure of the welded seam was characterized by optical microscopy (OM), scanning electron microscopy (SEM), X-ray diffraction (XRD), and energy dispersive spectrometer (EDS). Mechanical properties of the welded seam were evaluated by microhardness. The corresponding mechanisms were discussed in detail. Results show that the laser welded seam have non-equilibrium solidified microstructures consisting of Cr–Ni–Fe–C austenite solid solution dendrites as the dominant and some fine and dispersed $Ni_3(Al,Ti)$ γ' phase as well as little amount of MC needle carbides and particles enriched in Nb, Ti and Mo distributed in the interdendritic regions, cracks originated from the liquation of the low melting points eutectics in the HAZ grain boundary are observed, the average microhardness of the welded seam and HAZ is higher than that of the base metal due to alloy elements' redistribution of the strengthening phase γ'.

1. Introduction

K418 is a precipitation-strengthened nickel-based superalloy which is widely used in hot sections of gas turbine engines due to its excellent elevated temperature strength and superior hot corrosion resistance. Unfortunately, the processing of superalloys can be problematic in practice, because of the lack of ductility displayed. This is especially applicable to welding, one of the most important manufacturing processes, particularly for parts in the combustor and compressor sections. It derives its high-temperature strength primarily from precipitation hardening by $Ni_3(Al,Ti)$ γ' phase. The alloy, like other γ' precipitation hardening alloy with total Al and Ti more than 6 wt%, is high susceptible to microfissuring on welding (Minlin et al., 2005). For the reason, electronic-beam welding or friction welding has been used traditionally for the welding of components in the gas turbine sector. But the electronic-beam welding process needs vacuum chamber and produces harmful X-rays. On the other hand, the prospect of totally encompassing huge components in a vacuum canopy in order to effect the welding is not practicable. As for the friction welding, low stress destruction are often occurred and welding defects are observed near the fusion zone usually and results in lower production efficiency (Du et al., 2003, 2004).

Laser welding is a high-energy density, low heat-input process with specific advantages over conventional fusion welding processes. These include high welding speed, narrow heat-affected zone, and low distortion, ease of automation, single-pass thick section capability and enhanced design flexibility. One of the many features of laser welding is the capability to weld without filler materials and it offers distinct advantages (Sun and Ion, 1995; Sun and Kuo, 1999; Wang et al., 2000; Mai and Spowage, 2004). Laser welding has recently received growing attention due to its special features

* *Corresponding author*. Tel.: +86 10 82544250.
E-mail address: gyu@imech.ac.cn (G. Yu).
0924-0136/$ – see front matter © 2008 Elsevier B.V. All rights reserved.
doi:10.1016/j.jmatprotec.2007.12.091

Table 1 – Chemical composition of K418 (wt.%)

C	0.08–0.16
Cr	11.5–13.5
Mo	3.8–4.8
Nb	1.8–2.5
Al	5.5–6.4
Ti	0.5–1.0
Zr	0.06–0.15
B	0.008–0.020
Mn	≤0.50
Si	≤0.50
P	≤0.015
S	≤0.010
Fe	≤1.0
Pb	≤0.001
Bi	≤0.0001
Ni	Bal.

and potential. In terms of weldability for metallic materials, Nd:YAG laser has various advantages, such as a high-energy absorption rate due to a low reflectivity, a high welding speed, and a low residual stress compared to CO_2 laser, so the application of Nd:YAG laser to weld metallic materials is steadily being increased, it has been widely implemented in industrial applications, e.g. in the automotive industry (Kuo and Lin, 2006). But presently, little work has been carried out to investigate on fusion region microstructure and welding defect of laser welding K418. In the paper, 5 mm thickness K418 is butt welding by Nd:YAG laser. Microstructure and hot crack mechanism of joint are investigated.

2. Experimental procedures

The material used was cast K418 nickel-based superalloy with thickness 5 mm. The chemical composition is given in Table 1. Before welding, any oxide layers and contamination were removed from the surfaces of the components, especially the surfaces needed welding were cleaned with acetone and then dried. Fifteen litres per minute flow of high purity argon gas was passed through the molten pool from both top and lateral sides to provide a protective environment for the sake of avoiding the reaction between the molten metals and ambient air and blow away plasma on the welded specimen surface.

Experiments of laser welding K418 were conducted on a 3 kW Nd:YAG laser materials processing systems with five-axes computer-numerical-controlled (CNC) working station without any filler metal. The employed parameters that could cause much crack in fusion region and heat-affected region were based on our previous work. The parameter is laser output power 3 kW, the welding velocity 15 mm/s and the defocus distance −1 mm. The whole laser welding system is illustrated in Fig. 1. After welding, no post-weld heat treatments were performed.

Metallographic samples were machined by electric discharging cutting, followed by mechanical milling and grinding to acquire the testing surface with roughness of 0.8 μm from the slight rough as-laser welding specimens. Metallographic samples of the base metals and the welded seam were prepared using standard mechanical polishing procedures and were etched in $HCl:HNO_3$ solution in volume ratio

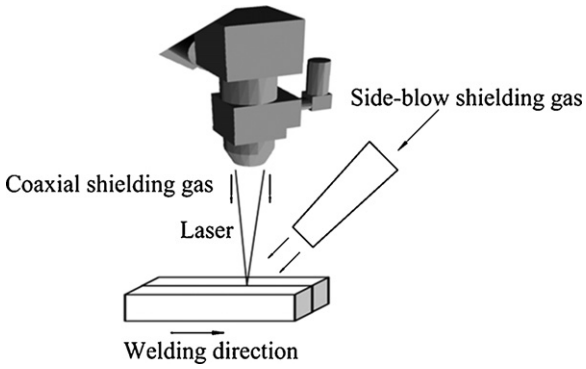

Fig. 1 – Schematic diagram of the experiment setup.

of 3:1. Microstructure of the welding seam was characterized by NephotIIoptical microscopy (OM), JSM-5800 scanning electron microscopy (SEM) equipped with LinkISIS S-530 energy-dispersive spectrometer (EDS). A D/max-rB high power multi-crystal X-ray diffractometer (XRD) was used for phase identification. The recorded intensities and peak positions were compared with Joint Committee on Powder Diffraction Standards (JCPDS) data. The hardness along the transverse direction of the welded seam was measured by an automatic microhardness tester (HXD-1000B, Shanghai Optics Apparatus Ltd., China) with a tested load of 1.96 N and a dwelling time of 15 s.

3. Experimental results and discussion

3.1. *Microstructure examinations*

The microstructure base metal (BM) consisted mainly of γ matrix with second phases of MC type carbides and γ+γ′ eutectic at the grain boundaries, as shown in Fig. 2. Average grain area in Figs. 2 and 3 is measured by using optical microstructure. Results show average grain areas of base metal and HAZ are 4919 and 6861 μm^2, respectively.

Fig. 4 shows the OM micrographs of the welded seam. Fig. 4a and b represents the microstructures of interface between welded seam and heat affected region and center of

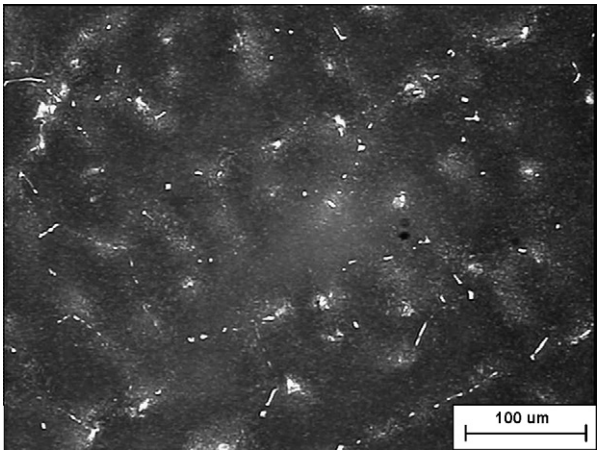

Fig. 2 – Microstructures of the base material.

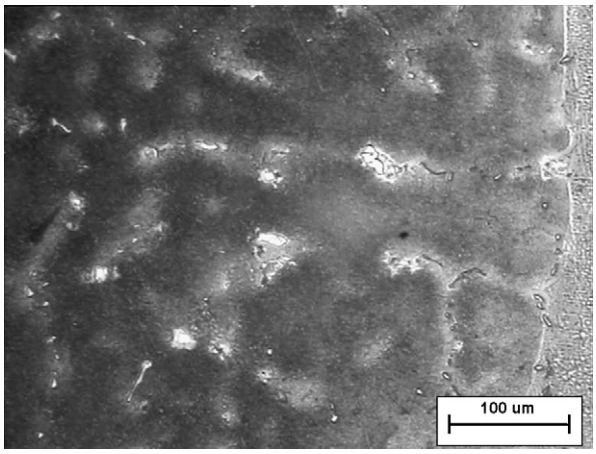

Fig. 3 – Microstructures of the HAZ.

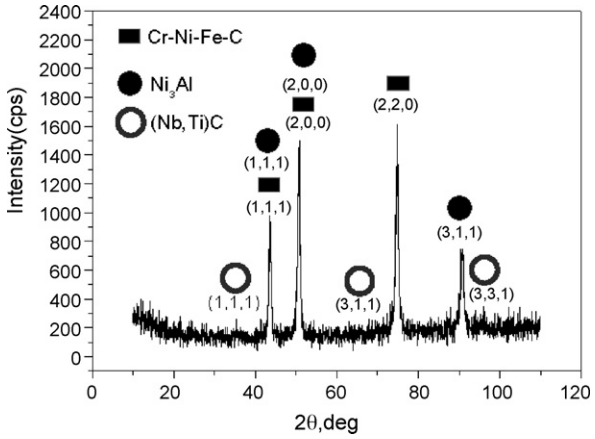

Fig. 5 – The X-ray diffraction result of the laser welded seam.

welded seam, respectively. It can be seen that the solidification microstructure is mainly composed of dendrites whose growing direction is nearly parallel to the negative heat-transfer direction, and the dendrites take on the shape of typical directional solidification microstructure from Fig. 4a. During the process of cooling solidification of the liquid metal, due to the cooling effect caused by the base metals, heat mostly dissipates in the normal direction of the interface, so the temperature gradient in this direction is remarkably dominant, which leads to the liquid metal holding the directivity. Under the action of the highest temperature gradient and solidification rate in the normal direction, grains grow with the directional selection, thus forming the dendrites, which are almost parallel to the negative normal direction.

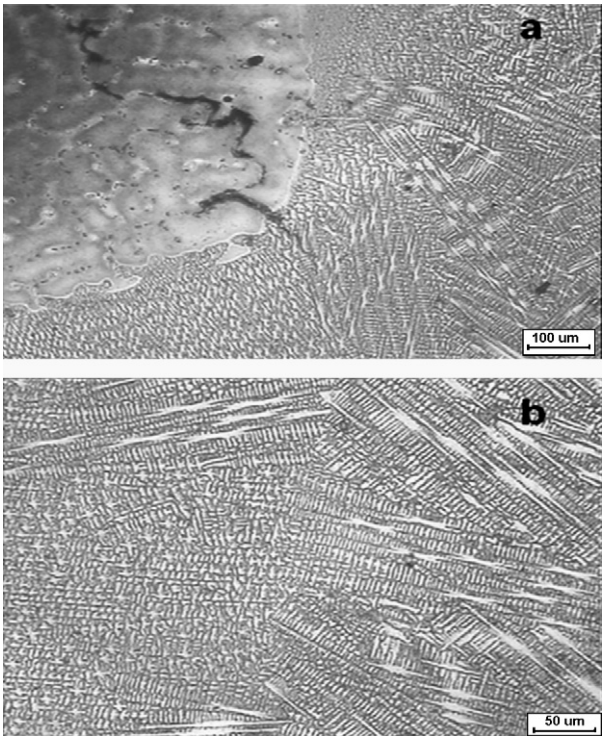

Fig. 4 – The microstructure of fusion region.

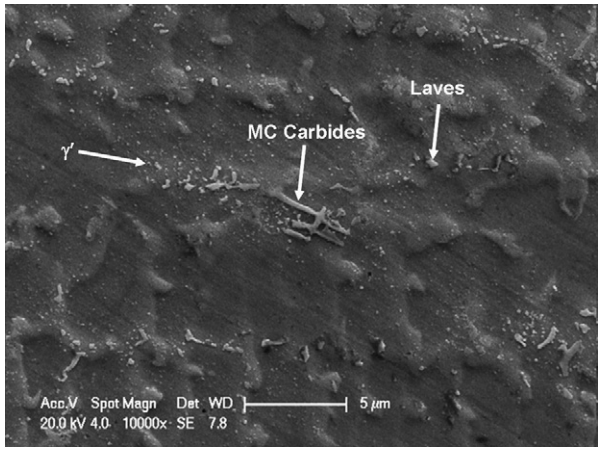

Fig. 6 – SEM microstructure of fusion region.

Fig. 5 demonstrates the X-ray diffraction result of the welded seam, from which it can be found that in the whole region of the welded seam, the peak of {111}, {200}, and {220} orientations is quite evident, which manifests that in the central region of the welded seam, the growing directions of grains are rather disorderly, and the solidification microstructure is not the directional solidification dendrite any longer.

At high magnifications, it can be seen from Fig. 6 that except the main dendrite structure, which identified by XRD as Cr–Ni–Fe–C austenite solid solution, and some fine and dispersed particles as $Ni_3(Al,Ti)$ γ' phase, some bright etching irregular-shaped particles and needle were seen in the interdendritic regions. EDS analysis of the needle is shown in Table 2, which indicates that needle are rich in Nb, Ti from Table 2, as enriched in Ti and Nb and confirmed as MC type (Ti, Nb)C carbides on account of the strong affinity of Ti and Nb with C in the melted pool. Reference (Zupanič et al., 2002) mentions that in the eutectic colonies the MC carbide possessed a skeletal morphology in which rod branching occurred very frequently in order to allow couple growth of MC and γ with high cooling rate. The EDS results obtained on these

Table 2 – EDS analysis results of the laser welded seam (Wt.%)

Major elements	Ni	Fe	Cr	Nb	Ti	Mo	Al
Dendrites core	76.14	0.29	12.23	0.86	0.62	4.06	5.79
Particles	64.36	0.47	12.50	9.14	1.95	7.03	4.54
Needle	66.92	0.38	12.30	6.93	1.65	6.62	5.20

particles is shown in Table 2, which indicates that these particles are enriched in Nb, Ti, Mo, and lean in Ni as compared to the austenite solid solution dendrites matrix. Chemical composition of the particles enriched in Nb was identified as (Fe + Cr + Ni, 77.33 wt%) and (Ti + Nb + Mo, 18.12 wt%). Considering their small particle size, electron probe microanalysis has a spot size of approximately one micrometer, which is larger than the particles size, resulting in the incorporation of the matrix material. Synthesizing the above results, the particles detected in the dendrites were quite similar to the Laves phase, which is a hexagonally close packed phase and is generally accepted to be of the form $(Ni, Cr, Fe)_2$(Nb, Mo and Ti) (Radhakrishna and Prasad Rao, 1997). Unfortunately, since Laves phase is heavily alloyed with multiple elements and its form is very complex as mentioned above, so, no present JCPDS cards could be found to identify the exact existence of it as indicated in Fig. 5. Maybe Transmission Electron Microscope (TEM) is a powerful tool to analyse the fine structure of it, this is our future work.

3.2. *HAZ liquation cracking*

The zig–zag morphology of the HAZ liquation cracks is observed in Fig. 7a. Fig. 7b is enlarged image of area marked in Fig. 7a A region. $M_{23}C_6$ particles and liquated MC carbides are observed in crack boundary from Fig. 7b (Ojo et al., 2004). EDS analysis of $M_{23}C_6$ particles and liquated MC carbides are shown in Figs. 8 and 9.

Heat-affected zone microfissuring is generally considered to be caused by the presence of low melting liquid on the grain boundaries. The liquid enables the boundaries to separate under the thermal and shrinkage stresses resulting from weld cooling cycle. It has, however, been recognized through many studies on liquation cracking that the mere occurrence of liquation is not sufficient to produce a crack susceptible microstructure. To incur cracking, continuous or semi-continuous grain boundary liquid should persist until a time when sufficient thermal and mechanical restraints have developed during cooling. In order to prevent crack initiation in heat affected zone during welding, it is necessary to reduce the welding heat-input for preventing low melting liquid, or rapid elimination of grain boundary liquid prior to the existence of sufficient level of tensile stresses would improve the alloy's resistance to liquation cracking.

3.3. *The microhardness of the laser welding seam*

The microhardness is an important index to evaluate the material properties. It depends on both the composition and the microstructure. Fig. 10 exhibits the microhardness distribution of the transverse of welded seam. It can be seen that

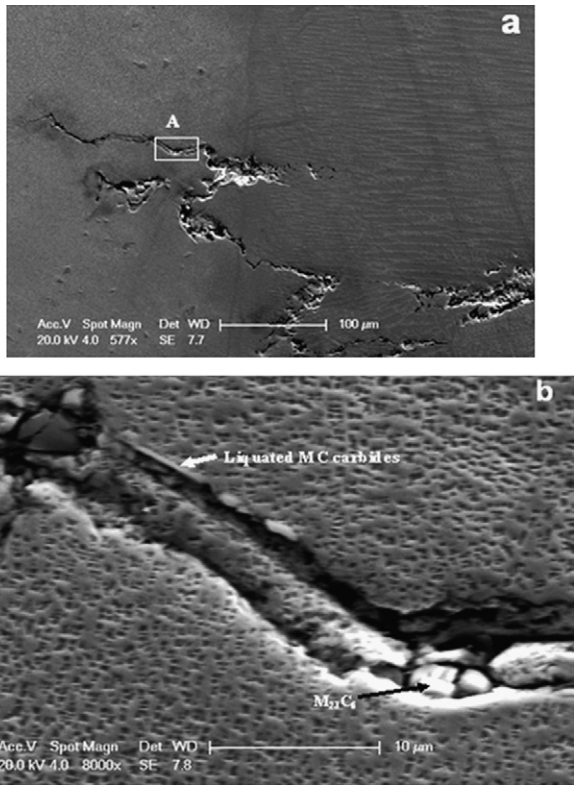

Fig. 7 – SEM liquated crack on the HAZ.

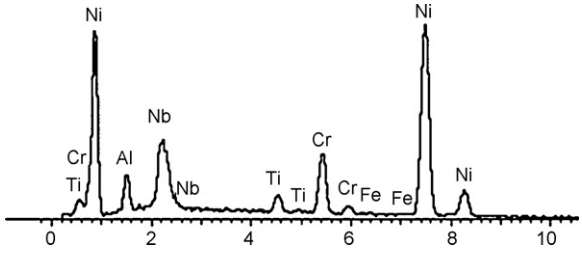

Fig. 8 – EDS spectrum from liquated MC carbides.

the hardness of welded seam is the highest, at about average HV397, the hardness of HAZ is about HV384, and then quickly changes to the base metal, about HV333.

The hardness results are important since weld strength mismatch is a major concern when welding most metallic materials. In practice, the weld may be stronger or weaker in comparison with the base materials. As a general rule, an

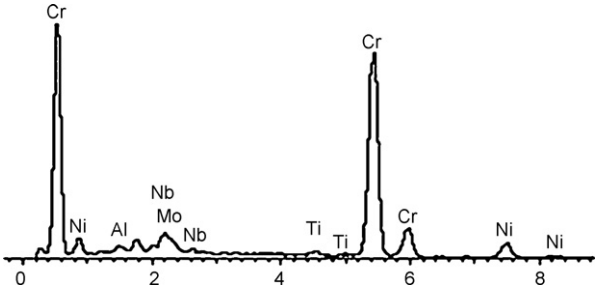

Fig. 9 – EDS spectrum from $M_{23}C_6$ particles.

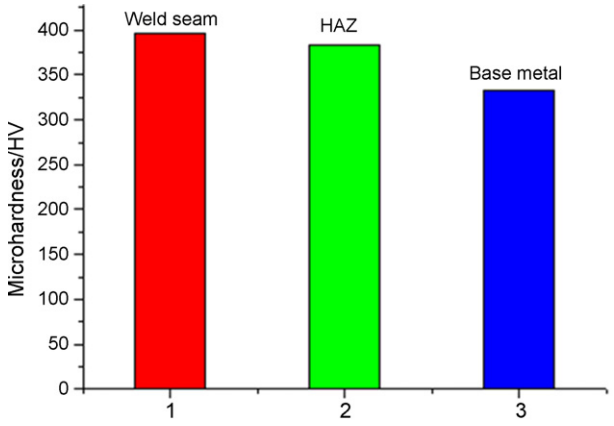

Fig. 10 – Microhadrness distribution from the welded seam to base metal.

attempt is made to design the weld to be stronger than the base materials. There is a possibility that could explain the differences of hardness from welded seam to base metal, which is the differences in the size and distributions of the strengthening phase $Ni_3(Al,Ti)$ γ′ caused among welded seam, HAZ and base metal by the melting and solidification of the material in fusion zone and welding peak temperature in HAZ (Sekhar and Read, 2002).

4. Conclusions

The microstructure and mechanical properties of laser welding cast nickel-based superalloy K418 have been investigated. Microstructure of the laser welded seam is mainly composed of Cr–Ni–Fe–C austenite solid solution dendrites as the dominant and some fine and dispersed $Ni_3(Al,Ti)$ γ′ phase as well as little amount of MC needle carbides and particles enriched in Nb, Ti and Mo distributed in the interdendritic regions. Laser welding nickel-based superalloy K418 demonstrates strong susceptibility to HAZ liquation cracks. Cracks originated from the liquation of MC carbides are observed. Mechanical tests show that the microhardness of the welded seam and HAZ are higher than the base metal due to the partial dissolution and alloy elements' redistribution of the strengthening phase γ′.

REFERENCES

Du, S.-G., Fu, L., Wang, J.-W., et al., 2003. Forming mechanism of carbide band in friction welding joint of superalloy K418 and steel 42CrMo. Chin. J. Nonferrous Metals 13 (2), 323.

Du, S.-G., Fu, L., Cao, Y., et al., 2004. On strengthening the friction welding joint between K418 Turbo disk and 42CrMo shaft. J. Northwest. Polytech. Univ. 22 (1), 112–115.

Kuo, T.Y., Lin, H.C., 2006. Effects of pulse level of Nd: YAG laser on tensile properties and formability of laser weldments in automotive aluminum alloys. Mater. Sci. Eng. A416, 281–289.

Mai, T.A., Spowage, A.C., 2004. Characterization of dissimilar joints in laser welding of steel–koval, copper–steel and copper–aluminium. Mater. Sci. Eng. A 374, 224–233.

Minlin, Z., Hongqing, S., Wenjin, L., et al., 2005. Boundary liquation and interface cracking characterization in laser deposition of Inconel 738 on directionally solidified Ni-based superalloy. Scripta Mater. 53 (2), 159.

Ojo, O.A., Richards, N.L., Chaturvedi, M.C., 2004. Liquation of various phases in HAZ during welding of cast Inconel 738LC. Mater. Sci. Technol. 20, 1032.

Radhakrishna, C.H., Prasad Rao, K., 1997. The formation and control of Laves phase in superalloy 718 welds. J. Mater. Sci. 32, 1977–1984.

Sekhar, N.C., Read, R.C., 2002. Power beam welding of thick section nickel base superalloys. Sci. Technol. Welding Joining 7 (2), 77–86.

Sun, Z., Ion, J.C., 1995. Review laser welding of dissimilar metal combinations. J. Mater. Sci. 30, 4205–4214.

Sun, Z., Kuo, M., 1999. Bridging the joint gap with wire feed laser welding. J. Mater. Process. Technol. 87, 213–222.

Wang, H.M., Chen, Y.L., Yu, L.G., 2000. 'In-Situ' weld-alloying/laser beam welding of SiCp/6061 Al MMC. Mater. Sci. Eng. A293, 1–6.

Zupanič, F., Bončina, T., Križman, A., Markoli, B., Spaič, S., 2002. Microstructural constituents of the Ni-based superalloy GMR 235 in the as-cast condition. Scripta Mater. 46, 670.